Adsorptive treatment via simultaneous removal of copper, lead and zinc from soil washing wastewater using spent coffee grounds

Cybelle M. Futalan, Jongsik Kim and Jurng-Jae Yee

ABSTRACT

In the present work, the performance of spent coffee grounds (SCG) as an adsorbent in the treatment of real soil washing wastewater (SWW) was evaluated. Scanning electron microscopy, Fourier transform infrared spectroscopy, zeta potential measurement and Brunauer–Emmett–Teller analysis were utilized to determine the physicochemical characteristics of SCG. Maximum removal efficiency of 68.73% for Cu(II), 57.23% for Pb(II) and 84.55% for Zn(II) was attained at 2.5 g SCG, 300 min and 328 K. Error analysis was performed using root mean square error (RMSE) and sum of square error (SSE). Equilibrium data correlated well with the Langmuir isotherm for Pb(II) adsorption and Freundlich model for the removal of Cu(II) and Zn(II). The kinetic study shows that adsorption of the heavy metals using SCG can be satisfactorily described using the pseudo-second order equation ($R^2 \geq 0.9901$; RMSE ≤ 15.0539; SSE ≤ 145.1461). Activation parameters including activation energy, change in free energy of activation, activation entropy change (ΔS^*) and activation enthalpy change (ΔH^*) were determined using Arrhenius and Eyring equations. Thermodynamic studies show that adsorption of the heavy metals using SCG is spontaneous, endothermic ($\Delta H^\circ \geq 9.80$ kJ/mol·K) and results in increased randomness at the solid/solution interface ($\Delta S^\circ \geq 2.28$ J/mol).

Key words | activation energy, error analysis, heavy metals, soil washing wastewater, spent coffee grounds, thermodynamics

Cybelle M. Futalan
National Research Center for Disaster-Free and Safe Ocean City,
Busan 49315,
Republic of Korea

Jongsik Kim
Department of Chemistry,
Dong-A University,
Busan 49315,
Republic of Korea

Jurng-Jae Yee (corresponding author)
Department of Architectural Engineering,
Dong-A University,
Busan 49315,
Republic of Korea
E-mail: *jjyee@dau.ac.kr*

INTRODUCTION

Heavy metal contamination in soil has been a challenging issue worldwide due to its detrimental effects on agricultural yield, human health, soil ecosystem and the aquatic environment especially groundwater reserves (Anawar *et al.* 2015). Heavy metals are naturally present in the earth's crust, and micronutrients such as copper and zinc are considered to be vital components needed by plants while lead does not have any significant function in biochemical processes (Suresh *et al.* 2016). The high quantity of heavy metals in the soil is due to their widespread application in various anthropogenic activities such as the electronics industry, burning of fossil fuels, fertilizer use, warfare and military training, pesticide use, smelting and mining industries, and production of municipal wastes (Kumar *et al.* 2017; Liu *et al.* 2018). Heavy metals enter the food chain via ingestion of affected crops and are known to cause a variety of diseases including chronic nephropathy, gastrointestinal irritation, liver cirrhosis, kidney and brain damage, renal failure and insomnia (Eisler 2000). Moreover, exposure of plants to high concentration of copper, lead and zinc could result in reduced transpiration and photosynthetic rate, DNA damage, decreasing soil microbial activity, phytotoxicity, and limited intercellular CO_2 concentration (Dinesh *et al.* 2012; Kumar *et al.* 2017).

Different *ex situ* remediation technologies are available in the management of contaminated soil including thermal desorption, soil washing, land farming, oxidation and base-catalyzed decomposition (Gomes *et al.* 2013). Soil washing has been extensively applied in several field or pilot-scale projects in Australia, European countries, Canada, USA and Korea (Liu *et al.* 2018) due to its satisfactory removal efficiency, lower capital costs and shorter duration of treatment (Wei *et al.* 2016). The technology employs a variety of leaching agents such as chelating solutions and inorganic and organic acids to extract pollutants from contaminated soil (Isoyama & Wada 2007). As a result, soil washing wastewater (SWW) is produced, which contains heavy metals and other

doi: 10.2166/wst.2019.087

contaminants, which would require proper treatment before it can be safely discharged into water bodies or sewer systems.

Numerous chemical and physical strategies have been employed in the treatment of SWW in order to remove organic and inorganic contaminants, including solar photocatalytic system (Onotri *et al.* 2017), electrolysis (dos Santos *et al.* 2015), adsorption (Makino *et al.* 2016; Feng *et al.* 2018) and photo-Fenton process (Bandala *et al.* 2008). Among the technologies, adsorption has been given considerable attention for wastewater treatment due to its ease of operation, capability of adsorbent reuse, technical flexibility, cost-effectiveness and high removal capacity (Ali *et al.* 2012; Dong *et al.* 2016). Recently, studies were conducted on the management of SWW via adsorption using alkali materials ($CaCO_3$, MgO, NaOH) and natural waste materials including tea residue, pineapple peel, broad bean straw and soybean straw (Makino *et al.* 2016; Feng *et al.* 2018). However, a literature review revealed that there have been no reports made on the possible use of coffee grounds in the treatment of real SWW. The application of synthetic solutions in the previous studies would not determine which parameters would affect the removal efficiency. Therefore, it is essential to employ real SWW to accurately assess and understand the mechanisms involved in the treatment method. In the present work, SWW was produced by treating contaminated soil with heavy metals using hydrochloric acid via a soil washing process.

Spent coffee grounds (SCG) refers to the residue generated by the manufacture of instant solubilized coffee where the ground coffee beans are roasted and steamed (Janissen & Huynh 2018). In Korea, an estimated 103,000 tonnes of SCG were generated in 2014 based on the report of the Korean Ministry of Environment (Kang *et al.* 2017). Several studies have investigated the added-value of SCG, including as a fuel (Silva *et al.* 1998) and as a low-cost adsorbent of dyes (Safarik *et al.* 2012) and heavy metals (Imessaoudene *et al.* 2016). The use of SCG as a viable material in wastewater remediation technology is associated with its availability in large quantities, being economical and having satisfactory adsorptive performance (Gomez-Gonzales *et al.* 2016). Application of agricultural or industry by-products in wastewater remediation is a sustainable approach to effectively reduce the disposal of solid waste in sanitary landfills or burning of waste via incinerators.

The present study evaluates the treatment of real SWW using SCG as an adsorbent in the simultaneous removal of copper, lead and zinc. The SCG were prepared via washing with deionized water and oven-drying, which would translate to minimal cost in adsorbent preparation. The physical and chemical characteristics of SCG were determined using scanning electron microscopy (SEM), Fourier transform infrared spectroscopy (FT-IR) and Brunauer–Emmett–Teller (BET) analysis. The activation and thermodynamic parameters were determined while experimental data were fitted using kinetic models such as pseudo-first order, pseudo-second order, intraparticle diffusion and film diffusion equations. Also, the isotherm behavior was evaluated using the Langmuir, Freundlich and Dubinin–Radushkevich (D-R) models. Based on literature, the wide application of linear regression in adsorption did not provide reliable results. Therefore, the present study utilized both linear and non-linear regression methods to evaluate the kinetic and isotherm parameters.

MATERIALS AND METHODS

Treatment of contaminated soil

Contaminated soil was collected from Busan, South Korea. Prior to treatment, soil samples were sieved to a size range less than 2.0 mm. About 50 mL of the extraction solution (0.1 M HCl) and 10 g of contaminated soil were mixed in a 125-mL Erlenmeyer flask for 6 h using a reciprocal shaker (8289U17, Boekel) at 90 rpm under room temperature. The slurry was allowed to settle for 4 h, after which the solution was filtered with a 0.8 μm filter (CHM Lab Group). After which, the supernatant was set aside for further treatment. The composition of SWW is illustrated in Table S1 (available with the online version of this paper). The initial metal concentration for Cu(II), Pb(II) and Zn(II) is 1060.00, 1911.00 and 303.12 mg/L, respectively.

Preparation of SCG

SCG were obtained from a local coffee shop located in Busan, South Korea. The SCG were washed using deionized water at 25 °C to remove dirt and color. The washing of the coffee residues was repeated several times until a colorless supernatant was attained. After which, SCG were dried in an oven (CDO Drying Oven, Chang Shin Scientific Co.) for 48 h at 65 °C and sieved; adsorbent with particle size range of 0.25 to 0.53 mm was utilized in the experimental runs.

Characterization of SCG

The surface area and other textural properties of the adsorbent was evaluated using a BET surface analyzer

(Micrometrics ASAP 2020, AutoChem II) at 77 K under N_2 atmosphere. The external surface of SCG was analyzed using SEM (JEOL JSM-6700F) at 10 kV. The functional groups of SCG before and after adsorption were identified using FT-IR (Nicolet 6700) within the 400 to 4,000 cm^{-1} range at a resolution of 4 cm^{-1}. Zeta potential measurements were carried out by adding 0.05 g SCG to 50 mL UV-sterilized double distilled water. The pH adjustment of the suspension was performed using 0.1 M HCl or NaOH. The zeta potential of the suspension was measured using a zeta potential analyzer (Zetasizer-2000ZS, Malvern Instruments) under varying pH (3.0 to 8.0).

Isotherm studies

Batch experiments were carried out where varying amount of SCG (0.5 to 4.0 g) was mixed with 50 mL SWW and agitated in a reciprocal shaker bath at 90 rpm under room temperature. Then, the solution was filtered and the residual metal concentration in the supernatant was analyzed using atomic absorption spectroscopy (AAS, AAnalyst 800, Perkin-Elmer). The adsorption capacity at any time t (q_t, mg/g) was computed using Equation (1):

$$q_t = \frac{(C_0 - C_t)}{M} \times V \tag{1}$$

where V is the volume of the SWW (mL), M is the adsorbent mass (g), C_0 and C_t are the initial concentration and concentration at any time t of the contaminant (mg/L), respectively.

Adsorption models including Langmuir, Freundlich and D-R isotherms were applied to describe the equilibrium of the adsorption system. The Langmuir model describes a monolayer adsorption occurring on a finite number of binding sites with similar energy levels (Langmuir 1918). The Langmuir equation is expressed as:

$$q_e = \frac{K_L q_{mL} C_e}{1 + K_L C_e} \tag{2}$$

where q_e is the adsorption capacity at equilibrium (mg/g), K_L is the Langmuir equilibrium constant (L/mg), q_{mL} is the maximum adsorption capacity (mg/g) and C_e is the adsorption capacity at equilibrium (mg/g).

The Freundlich model is based on an empirical relationship wherein an indefinite increase of the quantity of contaminant adsorbed occurs with the increasing concentration of contaminant present in the solution. The model can be defined by Equation (3):

$$q_e = K_F C_e^{1/n} \tag{3}$$

where K_F and n are Freundlich constants that refer to the adsorption capacity (mg/g) and adsorption intensity of the contaminant onto the adsorbent (g/L), respectively (Freundlich 1906).

The D-R isotherm is utilized in the assessment of the adsorption process, whether it is physical or chemical in nature (Matouq *et al.* 2015). The D-R model is as follows:

$$q_e = q_{DR} \exp\left(-K_{DR}\left[RT \ln\left(1 + \frac{1}{C_e}\right)\right]^2\right) \tag{4}$$

where q_{DR} refers to the theoretical saturation adsorption capacity (mg/g), K_{DR} is a D-R constant related to the energy of adsorption (mol^2/J^2), T is the operating temperature (K) and R is the universal gas constant (8.3145 J/mol·K) (Dubinin & Radushkevich 1947). The mean energy of adsorption (E_{DR}, kJ/mol) can be calculated using Equation (5):

$$E_{DR} = \frac{1}{\sqrt{2K_{DR}}} \tag{5}$$

Kinetic studies

Kinetic experiments were performed by adding 50 mL SWW and 2.5 g SCG to a 125-mL Erlenmeyer flask that was agitated at pre-determined time intervals (1 to 360 min) using 90 rpm. Then, the treated solution was filtered and the residual metal concentration was analyzed.

To determine the rate-determining step of the adsorption system, kinetic equations including pseudo-first order, pseudo-second order, intraparticle diffusion and film diffusion models were utilized. The pseudo-first order or Lagergren equation is expressed as:

$$q_t = q_e(1 - e^{-k_1 t}) \tag{6}$$

where k_1 is the rate constant of the pseudo-first order (min^{-1}) (Lagergren 1898).

The pseudo-second order equation is defined as a system where the square of the number of available binding sites corresponds to the adsorption rate (Ho & McKay 1999), which is provided as:

$$q_t = \frac{k_2 q_e^2 t}{1 + k_2 q_e t} \tag{7}$$

where k_2 refers to the rate constant derived from the pseudo-second order equation (g/mg·min).

The intraparticle diffusion equation is dependent on both time and adsorption capacity, and is represented by:

$$q_t = k_{id}t^{0.5} + C \tag{8}$$

where k_{id} is the rate constant of the intraparticle diffusion equation (mg/g·min$^{0.5}$) and C refers to the thickness of the boundary layer surrounding the adsorbent (mg/g) (Weber & Morris 1963).

The film diffusion model is expressed as Equation (9) (Boyd *et al.* 1947):

$$\ln(1 - F) = -k_{fd}t \tag{9}$$

$$F = \frac{q_t}{q_e} \tag{10}$$

where F refers to the fractional attainment at equilibrium and k_{fd} (min^{-1}) represents the rate constant.

Thermodynamic studies

Experimental runs were performed by agitating 2.5 g SCG and 50 mL SWW under varying temperature (288 to 328 K) under contact time of 300 min at 90 rpm. The feasibility of the adsorption system can be evaluated by determining the thermodynamic quantities including ΔG°, ΔH°, ΔS°, activation energy (E_a), ΔG^*, ΔH^* and ΔS^*.

The Arrhenius equation (Equation (11)) is utilized in determining the activation energy:

$$\ln k_2 = \ln A - \frac{E_a}{RT} \tag{11}$$

where E_a (kJ/mol) refers to the activation energy and A is the Arrhenius frequency collision factor (Tran *et al.* 2016). The value of E_a would indicate whether the governing mechanism of adsorption is physical ($E_a \leq$ 40 kJ/mol) or chemical ($E_a >$ 40 kJ/mol) (Boparai *et al.* 2011).

Thermodynamic activation parameters including change in free energy of activation (ΔG^*, kJ/mol), activation entropy change (ΔS^*, J/mol•K) and activation enthalpy change (ΔH^*, kJ/mol) define whether an activated complex is formed in the transitional state during adsorption (Petrou & Economou-Eliopoulos 2009). The ΔG^* can be expressed as Equation (12) while the Eyring equation (Equation (13)) was used to compute ΔH^* and ΔS^*:

$$\Delta G* = \Delta \mathrm{H}* - \mathrm{T}\Delta \mathrm{S}* \tag{12}$$

$$\ln\frac{k}{T} = \left(\ln\frac{k_B}{h} + \frac{\Delta S*}{R}\right) - \frac{\Delta H*}{RT} \tag{13}$$

where k_B refers to the Boltzmann constant (1.3807×10^{-23} J/K), k is the rate constant and h is the Planck constant (6.6261×10^{-34} J·s).

The change in adsorption free energy (ΔG°, kJ/mol), change in enthalpy (ΔH°, kJ/mol·K) and change in entropy (ΔS°, J/mol) can be calculated using Equations (14)–(16):

$$\Delta G^0 = -RT\ln\left[\frac{K_L}{\gamma_e}(1\,mol{\bullet}L^{-1})\right] \tag{14}$$

$$\log\gamma_e = -z^2 I_e^{1/2} \tag{15}$$

$$\ln\left[\frac{K_L}{\gamma_e}(1\,mol{\bullet}L^{-1})\right] = \frac{\Delta S^0}{R} - \frac{\Delta H^0}{RT} \tag{16}$$

where z is the charge of the contaminant, γ_e is the activity coefficient at equilibrium and I_e is the ionic strength of heavy metal ion at equilibrium (Liu 2009). Equation (15) takes into consideration that the contaminants involved are charged species present at high concentration.

Error analysis

Error functions including root mean square error (RMSE) and sum of square error (SSE) were utilized to measure the goodness of fit of the isotherm and kinetic models in correlation with the experimental data. The SSE and RMSE are expressed as:

$$\mathrm{SSE} = \sum_{i=1}^{p}\sum_{j=1}^{n_i}\left(q_{e,theor}^{ij} - q_{e,expl}^{i}\right)^2 \tag{17}$$

$$\mathrm{RMSE} = \sqrt{\frac{1}{n-1}\sum_{i=1}^{n}\left(q_{e,theor}^{i} - q_{e,expl}^{i}\right)^2} \tag{18}$$

where $q_{e,expl}^{i}$ corresponds to the measured concentration (mg/L), n is the number of data points in each run, p is the number of experiments under certain conditions, and $q_{e,theor}^{i}$ refers to the predicted value of the model (mg/L) (Gomez-Gonzales *et al.* 2016). Linear regression analysis was applied to determine the kinetic and isotherm parameters. Meanwhile, the solver add-in tool in Microsoft Excel was employed in evaluating the constants

derived from non-linear models, where the tool applies a programming method called the generalized reduced gradient algorithm.

RESULTS AND DISCUSSION

Characterization of SCG

In Figure 1(a) and 1(b), the surface morphology of SCG indicates an irregular, non-smooth surface filled with cavities and channels. This is advantageous since the presence of cavities would imply accessibility to the pore network of adsorbent material and higher surface area, which could lead to better adsorption capacity. Based on Figure 1(c), the N_2 adsorption/desorption shows a classic type IV isotherm with a hysteresis loop that implies SCG to be a mesoporous material. The measured BET surface area, total pore volume and average pore diameter were determined to be 1.06 m^2/g, 0.00785 cm^3/g and 9.56 nm, respectively. As illustrated in Figure 1(d), results indicate that the point of zero charge of SCG occurred approximately at pH 4.78. This implies that under acidic conditions ($pH < 4.78$), the surface of SCG is positively charged, while a basic pH would indicate the adsorbent surface to be deprotonated. The pH of the SWW was measured to be 5.67 ($pH_{SWW} > pH_{pzc}$), where the predominantly negatively charged surface of SCG favors the removal of positively charged Cu(II), Pb(II) and Zn(II) via electrostatic attraction.

The FT-IR spectra before and after adsorption of Cu(II), Pb(II) and Zn(II) are illustrated in Figure 1(e). In pure SCG, the peak observed at 3,433 cm^{-1} corresponds to the stretching vibration of hydroxyl (-OH) groups due to the presence of water molecules, alcohols and phenols. The bands at 2,848 and 2,916 cm^{-1} are due to the stretching vibrations of the asymmetric and symmetric –CH aliphatic chains of the methylene and methyl groups. Several bands including 1,630, 1,364, 1,108 and 1,022 cm^{-1} are due to stretching of –NH in secondary amine, stretching of hydroxyl (-OH) and amine (-NH) groups, vibration of C-O-C, and stretching vibration of C-OH groups, respectively (Imessaoudene *et al.* 2016). After adsorption, the bands were observed to become weak and less intense. Peaks at 3,433, 1,664 and 1,378 cm^{-1} shifted to 3,454, 1,643 and 1,383 cm^{-1}, respectively. This shows that hydroxyl (-OH), amine (-NH) and carbonyl (-C=O) groups present in SCG are involved in the removal of Cu(II), Pb(II) and Zn(II).

Effect of mass of adsorbent, contact time and temperature

In Figure 2(a), increasing the adsorbent mass from 0.1 to 2.5 g resulted in a corresponding increase in the removal efficiency from 32.12% to 57.32% for Cu(II), 21.34% to 45.99% for Pb(II) and 46.92% to 72.12% for Zn(II). The enhanced removal efficiency with higher adsorbent mass could be attributed to the increase in surface area and higher number of binding sites available on the adsorbent. The maximum removal efficiency of Cu(II), Pb(II) and Zn(II) was determined to be 57.32%, 45.99% and 72.12%, respectively, with an adsorbent mass of 2.5 g. It was observed that further increasing the adsorbent mass to 4.0 g showed no significant change in the removal efficiency of the three contaminants. Agglomeration of the adsorbent material occurs at high dosage, which could lead to reduced surface area and less binding sites exposed for adsorption.

As depicted in Figure 2(b), removal efficiency of 25.11%, 11.87% and 36.54% was attained within 15 min for Cu(II), Pb(II) and Zn(II), respectively. Initially, there is a high number of available binding sites that suggests the occurrence of external diffusion and adsorption of heavy metals onto the adsorbent surface. As the contact time was further increased, the removal efficiency was observed to gradually increase until equilibrium was attained at 180 min for Zn(II) and 300 min for Cu(II) and Pb(II). The maximum removal of 54.92%, 44.50% and 75.24% was obtained at equilibrium for Cu(II), Pb(II) and Zn(II), respectively. Adsorption at a longer contact time would indicate that heavy metals have to diffuse slowly into the pores of SCG due to the deficit of available binding sites. Moreover, the heavy metals would have difficulty in attaching onto the few available sites for adsorption due to the repulsive forces exerted between the heavy metal ions present in the bulk solution and adsorbed contaminants on the solid adsorbent (Ahmad & Rahman 2011). After equilibrium was attained, only a slight increase in removal efficiency was observed when the contact time was further increased to 360 min.

As seen from Figure 2(c), the removal percentage increases as the temperature was increased from 288 to 328 K. Among the contaminants, Zn(II) proved to have the highest removal rate in comparison to Cu(II) and Pb(II). At 328 K, the maximum removal efficiency of 68.73% for Cu(II), 57.23% for Pb(II) and 84.55% for Zn(II) was attained. This denotes that adsorption of Cu(II), Pb(II) and Zn(II) onto SCG is endothermic in nature. An adsorption system with higher temperature would signify higher kinetic energy that would cause better diffusion rate of the contaminants from

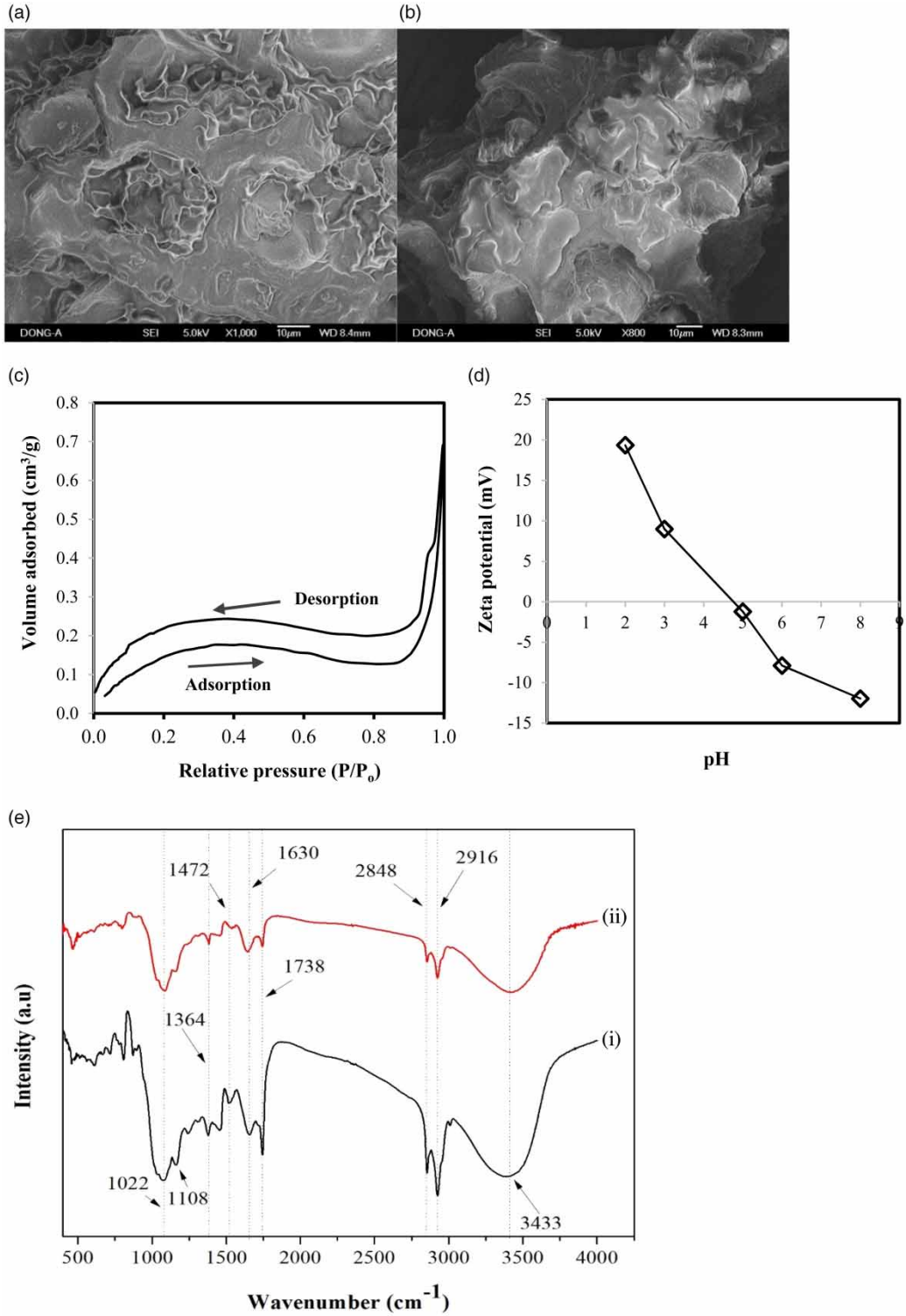

Figure 1 | Characterization of SCGs including SEM micrographs at magnification of (a) 1000x and (b) 800x, (c) N_2 sorption isotherm, (d) zeta potential values under varying pH and (e) FT-IR spectra before (i) and after (ii) adsorption.

the bulk to the adsorbent surface (Gode & Pehlivan 2005). Moreover, there would be an enhanced collision frequency between the contaminants and adsorbent surface that would lead to better adsorption (Saini & Melo 2013).

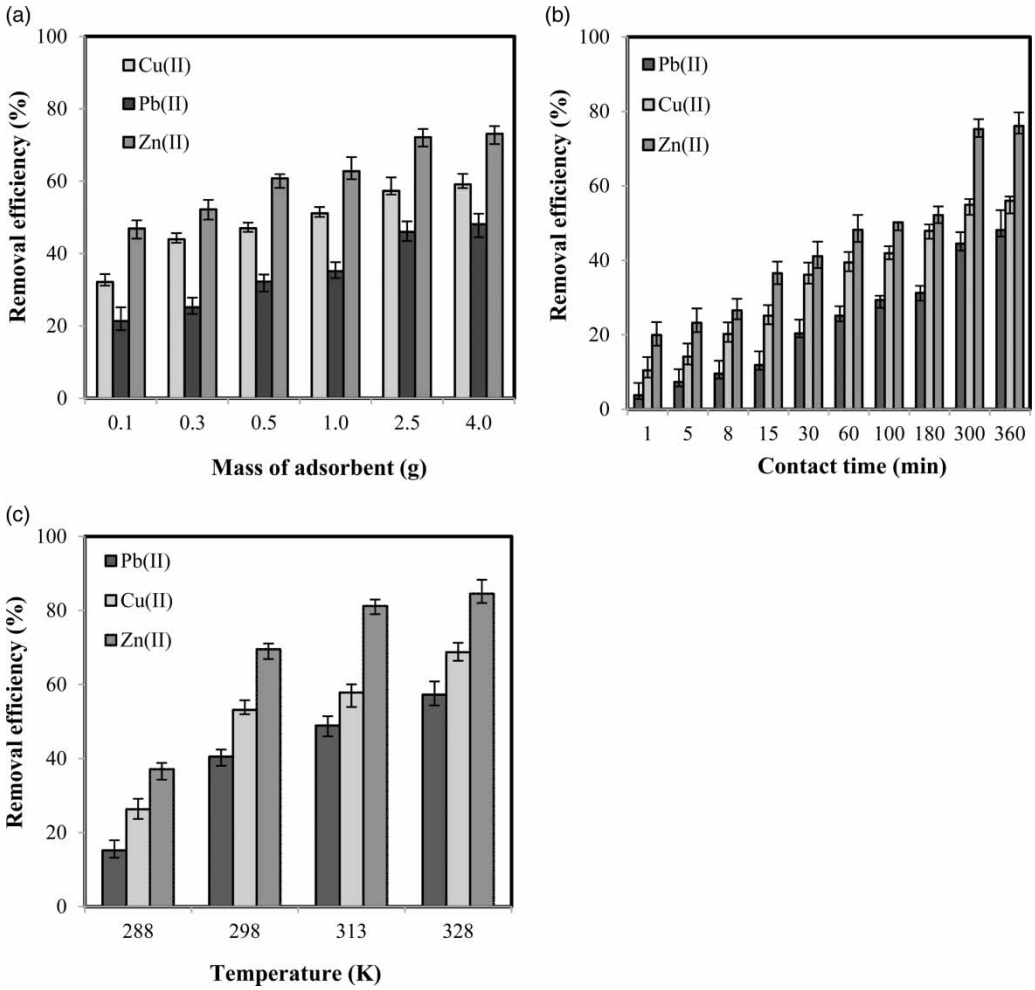

Figure 2 | The effect of (a) adsorbent mass (temperature = 298 K; contact time = 300 min), (b) contact time (temperature = 298 K; adsorbent mass = 2.5 g) and (c) temperature (contact time = 300 min; adsorbent mass = 2.5 g) on the removal efficiency of Cu(II), Pb(II) and Zn(II) from SWW using SCG.

Kinetic study

Table 1 shows the kinetic parameters derived from the pseudo-first order, pseudo-second order, intraparticle diffusion and film diffusion equations while Figure 3 illustrates the linear plots of the kinetic models. Low values of R^2 and high values of RMSE and SSE for pseudo-first order, intraparticle diffusion and film diffusion equations imply that the models were not suitable in describing the adsorption system using SCG. For the intraparticle diffusion equation (Figure 3(a)), the plot lines indicate the occurrence of two diffusion stages. The steeper (near the origin) plot slope is attributed to film diffusion while the later flatter slope represents intraparticle diffusion. Based on the k_{id} values ($k_{id1} > k_{id2}$), film diffusion occurs at a faster rate than intraparticle diffusion.

Results show that the pseudo-second order equation has highest coefficient of determination values ($R \geq 0.9901$) and low values of RMSE ($5.9911 \leq \text{RMSE} \leq 15.0539$) and SSE ($45.0974 \leq \text{SSE} \leq 145.1461$). When compared to the linear regression method, the lowest values of RMSE and SSE and highest R^2 values generated by the non-linear analysis imply it is a better approach in estimating the kinetic parameters. Based on Figure 3(c), experimental data fitted well with the linear plot generated by the pseudo-second order equation. Therefore, the adsorptive removal of Cu(II), Pb(II) and Zn(II) from SWW using SCG can be accurately described using the pseudo-second order model. This is further validated where the $q_{e,theo}$ values generated by the pseudo-second order equation are in good agreement with the experimental values of q_e ($q_{e,expl} = 18.36$ mg/g Pb(II); $q_{e,expl} = 13.75$ mg/g Cu(II); $q_{e,expl} = 2.66$ mg/g Zn(II)). Results denote that chemisorption is the rate-determining step wherein a covalent bond is formed between heavy metal ions and binding sites of SCG. The values of k_2 can be arranged in the order: Zn(II) > Cu(II) > Pb(II), wherein

Table 1 | Kinetic parameters of the adsorption of Cu(II), Pb(II) and Zn(II) from SWW using SCGs at 25 °C obtained from non-linear and linear regression analysis

		Contaminant					
		Cu(II)		Pb(II)		Zn(II)	
Kinetic model	Parameter	Linear	Non-linear	Linear	Non-linear	Linear	Non-linear
Pseudo-first order	k_1	0.0207	0.0187	0.0203	0.0176	0.0175	0.0151
	$q_{e(theo)}$	0.92	1.13	3.97	4.78	0.22	0.63
	R^2	0.9865	0.9701	0.9870	0.9633	0.9669	0.9709
	RMSE	21.0563	11.4710	18.7420	9.2201	16.2063	8.0900
	SSE	189.0495	143.8759	201.2662	105.8870	171.1560	87.3440
Pseudo-second order	k_2	0.0188	0.0213	0.0167	0.0196	0.484	0.603
	$q_{e(theo)}$	2.74	2.80	12.85	13.99	18.55	20.11
	R^2	0.9901	0.9957	0.9993	0.9944	0.9964	0.9987
	RMSE	12.6468	8.0291	15.0539	9.0116	8.7459	5.9911
	SSE	127.9005	45.0974	145.1461	71.0331	87.2983	55.0366
Intraparticle diffusion	k_{id1}	7.9739	5.4812	15.0640	13.0331	3.3138	1.5718
	k_{id2}	3.7917	1.0254	3.6935	2.7952	0.7573	0.8953
	R^2	0.9749	0.9811	0.9856	0.9889	0.8309	0.8596
	RMSE	32.0098	15.2384	22.2834	14.0406	20.1409	8.1121
	SSE	198.0751	131.4165	223.4406	195.4769	180.6718	166.2211
Film diffusion	k_{fd}	0.0111	0.0098	0.0147	0.0672	0.0081	0.0175
	R^2	0.9537	0.9331	0.9614	0.9755	0.9455	0.9487
	RMSE	66.9193	48.9102	54.2930	40.2189	73.8273	51.8302
	SSE	192.7210	140.8372	178.7291	122.9831	200.9182	162.9102

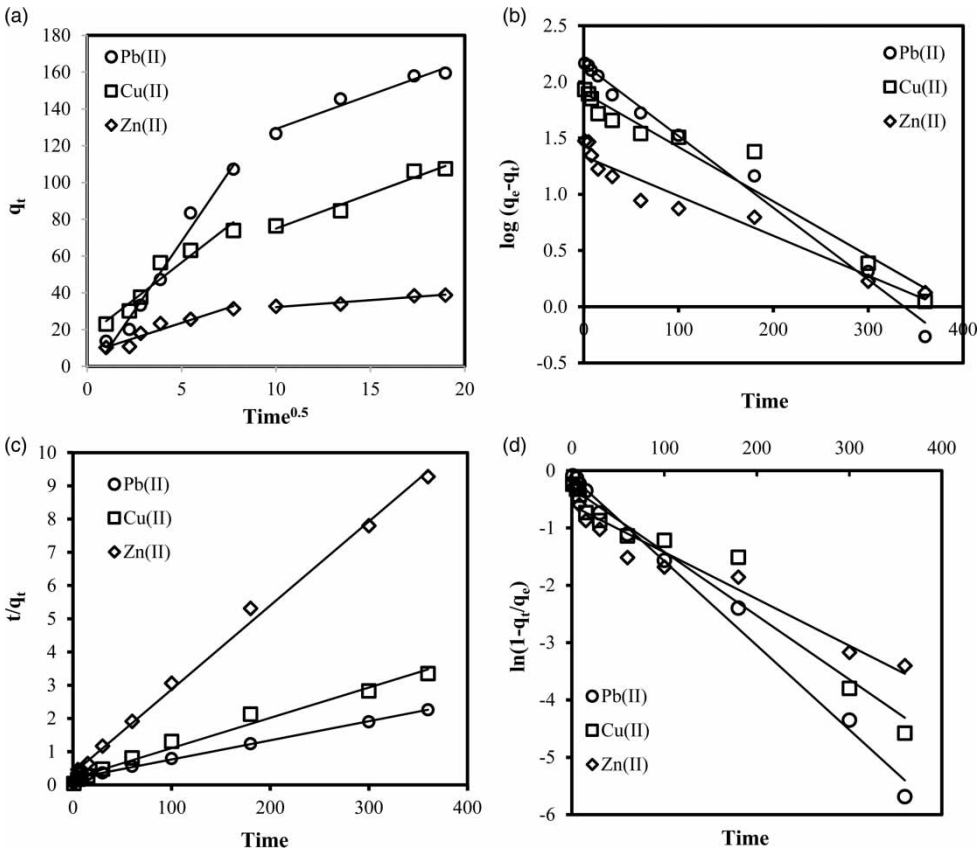

Figure 3 | Linear plots of (a) intraparticle diffusion, (b) pseudo-first order, (c) pseudo-second order and (d) film diffusion equations for the adsorption of Cu(II), Pb(II) and Zn(II) onto SCG.

a high rate constant is attributed to the small hydrated ionic radius of Cu(II) and Zn(II) that resulted in higher adsorption rates and favorable removal efficiencies.

Thermodynamic study

The activation parameters that define the activated complex (otherwise known as a transition-state complex) formed during the transition state of the adsorption process are derived from the Erying plot (Figure S1(a)) (Figure S1 is available with the online version of this paper). Based on Table 2, the positive value of ΔH^* for all three metals indicates the reaction to be of endothermic nature. A negative value of ΔS^* implies that adsorption of Cu(II), Pb(II) and Zn(II) onto SCG occurs via an associative mechanism (Mohapatra *et al.* 2009). This indicates that the activated complex takes on a more ordered and rigid structure when compared to the reactants. The low value of ΔS^* could be attributed to the adsorption of contaminants onto adsorbent or formation of bonds, where a decrease in the degree of freedom occurs during the transition phase (Petrou 2012). Under the temperature range studied, ΔG^* values are positive suggesting that energy is required to convert the reactants into activated complexes (Chowdhury *et al.* 2011).

Table 3 provides the thermodynamic parameters and E_a values that were derived from the van 't Hoff (Figure S1(b)) and Arrhenius (Figure S1(c)) plots, respectively. Based on the E_a values, the predominant mechanism of adsorption for Pb(II), Cu(II) and Zn(II) is physisorption. The negative ΔG° values of heavy metals indicate that adsorption is spontaneous and feasible from 288 to 328 K. As the temperature was increased, ΔG° value becomes more negative that denotes adsorption is more favorable at 328 K. The positive value of ΔH° suggests the adsorption process to be endothermic where higher values of adsorption capacity would be attained at higher temperature. Based on the magnitude of the ΔH° values, the governing adsorption mechanism is purely a physical process where the removal of heavy metals using SCG suggests involvement of weak forces of attraction. Results show that ΔS° has a positive value, which shows an increased randomness occurring at the adsorbent/contaminant interface. This is attributed to the release of solvated water molecules by the hydrated metal ions and SCG surface (Panda *et al.* 2018).

Table 2 | Activation parameters for the multi-metal adsorption of Cu(II), Pb(II) and Zn(II) using SCG

Metal	Temperature (°C)	ΔG^* (kJ/mol)	ΔH^* (kJ/mol·K)	ΔS^* (J/mol)
Pb(II)	15	80.40	9.29	−246.81
	25	82.87		
	40	86.57		
	55	90.28		
Cu(II)	15	80.30	22.34	−201.13
	25	82.31		
	40	85.33		
	55	88.34		
Zn(II)	15	72.15	12.02	−208.65
	25	74.23		
	40	77.36		
	55	80.49		

Table 3 | Thermodynamic parameters for the multi-metal adsorption of Cu(II), Pb(II) and Zn(II) using SCG

Metal	Temperature (°C)	E_a (kJ/mol)	ΔG° (kJ/mol)	ΔH° (kJ/mol·K)	ΔS° (J/mol)
Pb(II)	15	11.84	−8.92	20.98	83.79
	25		−11.69		
	40		−11.91		
	55		−15.66		
Cu(II)	15	24.90	−10.29	9.80	2.28
	25		−10.68		
	40		−11.40		
	55		−11.62		
Zn(II)	15	14.58	−7.30	16.58	28.91
	25		−7.82		
	40		−8.52		
	55		−9.06		

Isotherm study

The isotherm model parameters of the removal of Cu(II), Pb(II) and Zn(II) using SCG are illustrated in Table 4. Based on high R^2 values and low RMSE and SSE values, results show that adsorption of Pb(II) follows the Langmuir isotherm while removal of Cu(II) and Zn(II) can be best described using the Freundlich isotherm. Moreover, the low values of RMSE and SSE with high values of R^2 for the non-linear regression method imply that it is more suitable than the linear regression model in describing the adsorption of the metals using SCG. It can be seen that the equilibrium data for Cu(II) and Zn(II) uptake have a better fit to the linear plot of the Freundlich isotherm while Pb(II) adsorption is in good agreement with the linear plot of Langmuir (Figure 4(a)–4(c)).

Based on the Langmuir isotherm, Pb(II) displayed the highest q_{mL} value followed by Cu(II) and Zn(II). Firstly, SWW contained a higher concentration of Pb(II), which implies a better concentration gradient that would help to overcome the mass transfer resistance existing between the

Table 4 | Adsorption isotherm parameters of the removal of Cu(II), Pb(II) and Zn(II) on SCGs obtained from non-linear and linear regression analysis

		Contaminant					
		Cu(II)		Pb(II)		Zn(II)	
Isotherm	Parameter	Linear	Non-linear	Linear	Non-linear	Linear	Non-linear
Langmuir	q_{mL} (mg/g)	21.34	24.28	46.29	48.13	4.98	5.25
	K_L (L/mg)	0.01566	0.02388	0.00819	0.00982	0.04555	0.06256
	R^2	0.8488	0.8610	0.9833	0.9892	0.6393	0.6943
	RMSE	19.1062	12.5620	12.6528	10.6807	28.9012	16.9977
	SSE	283.4599	142.2370	167.1883	119.8222	248.1228	199.4787
Freundlich	K_F (mg/g)	13.24	10.96	18.90	17.65	4.47	5.88
	n (g/L)	0.1147	0.1029	0.1309	0.1685	0.0914	0.0852
	R^2	0.9289	0.9461	0.9144	0.9333	0.9394	0.9474
	RMSE	7.4788	6.3049	21.0511	19.9740	10.2292	8.0030
	SSE	109.8113	77.8974	237.1653	127.7748	160.6328	145.9153
D-R	q_{DR} (mg/g)	17.25	19.3013	35.93	36.3208	6.39	8.0288
	E_{DR} (kJ/mol)	6.20	7.59	7.88	9.04	2.18	4.27
	R^2	0.9075	0.9133	0.8861	0.9003	0.9061	0.9294
	RMSE	12.4417	10.0139	27.3866	25.5215	14.7221	12.0453
	SSE	140.4825	116.5572	208.1559	174.1330	302.2944	245.5528

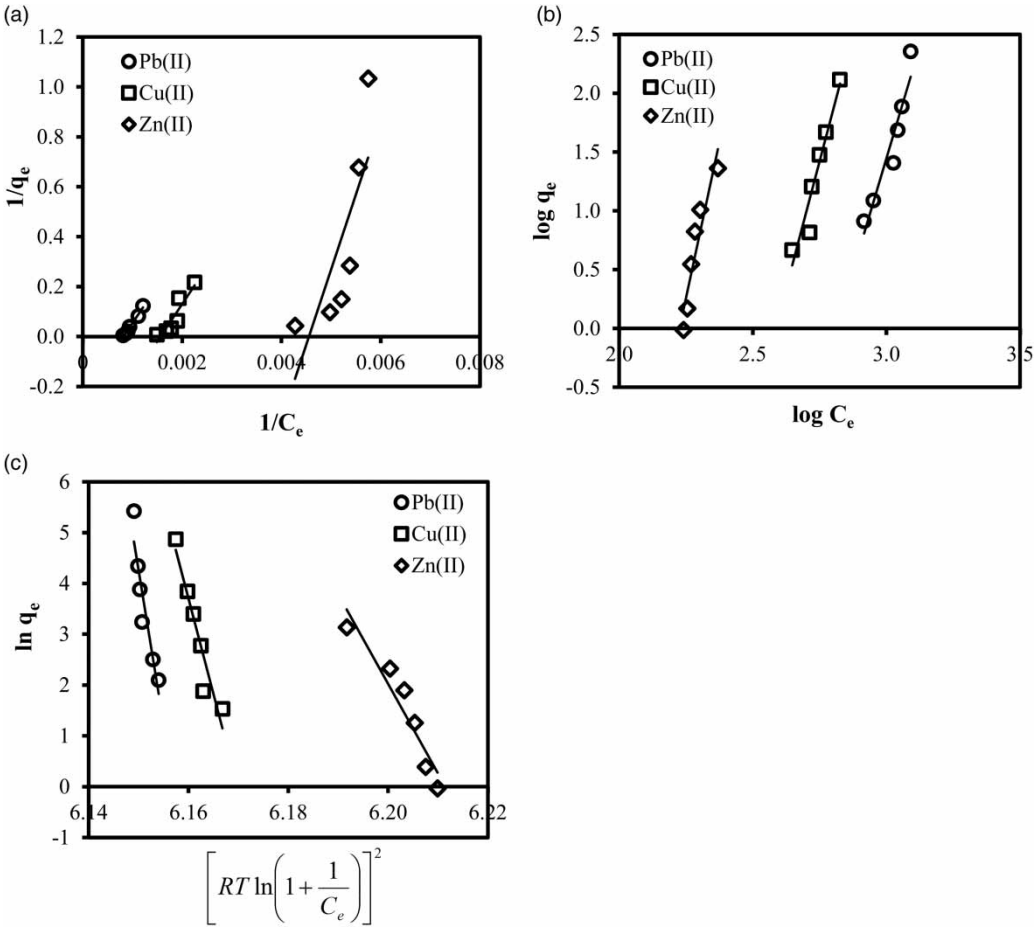

Figure 4 | Isotherm plots for (a) Langmuir, (b) Freundlich and (c) D-R model for the adsorption of Cu(II), Pb(II) and Zn(II) onto SCG.

liquid and solid phases and would result in higher value of adsorption capacity. In addition, the sequence of adsorption capacity of the contaminants is also related to metal properties including electronegativity, hydrolysis constant and softness value. Electronegativity of a metal ion is the ability to attract electrons towards itself to form a bond with another atom or ion. There is more attraction between two atoms or molecules when their electronegativity difference is large (Virjayaghavan *et al.* 2009). On the other hand, a smaller value of hydrolysis constant indicates that the metal ion easily forms a hydroxo-complex that is preferably adsorbed over the free metal cations. In addition, a large softness value denotes that the ion has a higher tendency to form electrostatic and inner sphere complexes with an adsorbent (Usman 2008). Based on the isotherm data, Pb(II) is preferentially adsorbed over Cu(II) and Zn(II) onto the adsorbent surface due to its high electronegativity, high softness value and easy hydrolysis.

Based on the Freundlich isotherm, the K_F values can be arranged in the order: Pb(II) > Cu(II) > Zn(II). This implies that Pb(II) has better adsorption capacity over Cu(II) and Zn(II). The n values of the heavy metals were determined to be less than 1, which indicates that the adsorption intensity is satisfactory over the entire concentration range studied. In the D-R isotherm, physical adsorption was determined to predominate the adsorption of heavy metals using SCG based on its E_{DR} values ($\leq$9.04 kJ/mol).

Table 5 compares the q_{mL} obtained for Cu(II), Pb(II) and Zn(II) in the present work with that of other adsorbents of previous studies in order to verify the viability of SCG as an adsorbent in the treatment of SWW. In addition, the BET surface area of the adsorbents is provided in Table 5. The highest adsorption capacity for Cu(II) was attained by cationic surfactant modified bentonite followed by SCG, while cucumber peel provided the highest q_{mL} value followed by SCG for the removal of Pb(II). Meanwhile, SiNTPP (silica chemically modified with porphyrin) provided a relatively high adsorption capacity over cationic surfactant modified bentonite and SCG for Zn(II) removal. A high surface area (SiNTPP and cationic surfactant modified bentonite) would yield high adsorption capacity for heavy metals, which means a greater number of binding sites are exposed to adsorb contaminants. Despite the low surface area of SCG, a satisfactory adsorption capacity was attained specifically for Cu(II) and Pb(II). Previous studies have mainly utilized aqueous solution where a single contaminant is present in the adsorption system. On the other hand, the present work employed real SWW comprised of a matrix of inorganic and organic contaminants that would lead to competitive effects and interference during the adsorption process.

CONCLUSION

In the present work, SCG as an adsorbent was evaluated in the uptake of Cu(II), Pb(II) and Zn(II) from real SWW. Based on high R^2 values and low RMSE and SSE values, equilibrium studies illustrate that adsorption of Pb(II) correlated well with the Langmuir isotherm while removal of Cu(II) and Zn(II) best fits the Freundlich model. Under the optimum condition of 2.5 g SCG, 300 min and 328 K, the maximum adsorption capacity at monolayer coverage for Cu(II), Pb(II) and Zn(II) was determined to be 24.28, 48.13 and 5.25 mg/g, respectively. The pseudo-second order equation was determined to adequately describe the experimental data, which denotes chemisorption as the rate-limiting step. In general, the kinetic and isotherm constants derived from the linear and non-linear approach showed marginal variation.

Table 5 | Comparison of the adsorption capacity of Cu(II), Pb(II) and Zn(II) using SCGs with other adsorbents

Metal	Adsorbent	BET surface area (m^2/g)	q_{mL} (mg/g)	Reference
Cu(II)	Cationic surfactant modified bentonite	15.57	50.76	Tohdee *et al.* (2018)
	Ceramsite	0.4967	5.39	Wang *et al.* (2018)
	SiNTPP	242.30	20.01	Radi *et al.* (2017)
	SCG	1.06	21.34	Present work
Pb(II)	SiNTPP	242.30	59.88	Radi *et al.* (2017)
	Cucumber peel	Not available	133.60	Basu *et al.* (2017)
	SCG	1.06	46.29	Present work
Zn(II)	SiNTPP	242.30	37.03	Radi *et al.* (2017)
	Cationic surfactant modified bentonite	15.57	35.21	Tohdee *et al.* (2018)
	Cocoa shell	Not available	2.90	Meunier *et al.* (2003)
	SCG	1.06	4.98	Present work

Thermodynamic studies revealed the adsorption process to be feasible, spontaneous and endothermic in nature, and results in an increased randomness at the solute/solid interface. Lastly, results of the present work illustrate the possible application of SCG as a low-cost, readily available adsorbent in removing Cu(II), Pb(II) and Zn(II) from real SWW.

ACKNOWLEDGEMENTS

The authors would like to acknowledge the National Research Foundation (NRF) of Korea through Ministry of Education (No. 2016R1A6A1A03012812) for the financial support of this research undertaking.

REFERENCES

Ahmad, M. A. & Rahman, N. K. 2011 Equilibrium, kinetics and thermodynamic of Remazol Brilliant Orange 3R dye adsorption on coffee husk-based activated carbon. *Chemical Engineering Journal* **170** (1), 154–161.

Ali, I., Asim, M. & Kahn, T. A. 2012 Low cost adsorbents for the removal of organic pollutants from wastewater. *Journal of Environmental Management* **113**, 170–183.

Anawar, H. M., Akter, F., Solaiman, Z. M. & Strezov, V. 2015 Biochar: an emerging panacea for remediation of soil contaminants from mining, industry and sewage wastes. *Pedosphere* **25** (5), 654–665.

Bandala, E. R., Velasco, Y. & Torres, L. G. 2008 Decontamination of soil washing wastewater using solar driven advanced oxidation processes. *Journal of Hazardous Materials* **160** (2–3), 402–407.

Basu, M., Guha, A. K. & Ray, L. 2017 Adsorption of lead on cucumber peel. *Journal of Cleaner Production* **151**, 603–615.

Boparai, H. K., Joseph, M. & O'Carroll, D. M. 2011 Kinetics and thermodynamics of cadmium ion removal by adsorption onto nano zerovalent iron particles. *Journal of Hazardous Materials* **186** (1), 458–465.

Boyd, G. E., Adamson, A. M. & Myers, L. S. 1947 The exchange adsorption of ions from aqueous solutions by organic zeolites. II. Kinetics. *Journal of the American Chemical Society* **63** (11), 2836–2848.

Chowdhury, S., Mishra, R., Saha, P. & Kushwaha, P. 2011 Adsorption thermodynamics, kinetics and isoteric heat of adsorption of malachite green onto chemically modified rice husk. *Desalination* **265** (1–3), 159–168.

Dinesh, R., Anandaraj, M., Srinivasan, V. & Hamza, S. 2012 Engineered nanoparticles in the soil and their potential implications to microbial activity. *Geoderma* **173–174**, 19–27.

Dong, C., Zhang, F., Pang, Z. & Yang, G. 2016 Efficient and selective adsorption of multi-metal ions using sulfonated cellulose as adsorbent. *Carbohydrate Polymers* **151**, 230–236.

dos Santos, E. V., Sáez, C., Martínez-Huitle, C. A., Cañizares, P. & Rodrigo, M. A. 2015 Combined soil washing and CDEO for the removal of atrazine from soils. *Journal of Hazardous Materials* **300**, 129–134.

Dubinin, M. M. & Radushkevich, L. V. 1947 The equation of the characteristic curve of the activated charcoal. *Proceedings of the USSR Academy of Sciences Physical Chemistry* **55**, 331–337.

Eisler, R. 2000 *Handbook of Chemical Risk Assessment: Health Hazards to Humans, Plants and Animals. Vol. 2: Organics*. Lewis Publishers, USA.

Feng, C., Zhang, S., Li, L., Wang, G., Xu, X., Li, T. & Zhong, Q. 2018 Feasibility of four wastes to remove heavy metals from contaminated soils. *Journal of Environmental Management* **212**, 258–265.

Freundlich, H. M. 1906 Over the adsorption in solution. *The Journal of Physical Chemistry* **57**, 385–470.

Gode, F. & Pehlivan, E. 2005 Adsorption of Cr(III) ions by Turkish brown coals. *Fuel Processing Technology* **86** (8), 875–884.

Gomes, H. I., Dias-Ferreira, C. & Ribeiro, A. B. 2013 Overview of in situ and ex situ remediation technologies for PCB-contaminated soils and sediments and obstacles for full-scale application. *Science of the Total Environment* **445–446**, 237–260.

Gomez-Gonzales, R., Cerino-Córdova, F. J., Garcia-León, A. M., Soto-Regalado, E., Davila-Guzman, N. E. & Salazar-Rabago, J. J. 2016 Lead biosorption onto coffee grounds: comparative analysis of several optimization techniques using equilibrium adsorption models and ANN. *Journal of the Taiwan Institute of Chemical Engineers* **68**, 201–210.

Ho, Y. S. & McKay, G. 1999 Pseudo-second order model for sorption processes. *Process Biochemistry* **34** (5), 451–465.

Imessaoudene, D., Hanini, S., Bouzidi, A. & Ararem, A. 2016 Kinetic and thermodynamic study of cobalt adsorption by spent coffee. *Desalination and Water Treatment* **57** (13), 6116–6123.

Isoyama, M. & Wada, S. 2007 Remediation of Pb-contaminated soils by washing with hydrochloric acid and subsequent immobilization with calcite and allophanic soil. *Journal of Hazardous Materials* **143** (3), 636–642.

Janissen, B. & Huynh, T. 2018 Chemical composition and value-adding applications of coffee industry by-products: a review. *Resources, Conservation and Recycling* **128**, 110–117.

Kang, S. B., Oh, H. Y., Kim, J. J. & Choi, K. S. 2017 Characteristics of spent coffee ground as a fuel and combustion test in a small boiler (6.5 kW). *Renewable Energy* **113**, 1208–1214.

Kumar, B., Smita, K. & Flores, L. C. 2017 Plant mediated detoxification of mercury and lead. *Arabian Journal of Chemistry* **10**, S2335–S2342.

Lagergren, S. Y. 1898 About the theory of so-called adsorption of soluble substances. *Kungliga Svenska Vetenskapsakademiens Handlingar* **24**, 1–39.

Langmuir, I. 1918 The adsorption of gases on plane surfaces of glass, mica and platinum. *Journal of the American Chemical Society* **40** (9), 1361–1403.

Liu, Y. 2009 Is the free energy change of adsorption correctly calculated? *Journal of Chemical and Engineering Data* **54** (7), 1981–1985.

Liu, L., Li, W., Song, W. & Guo, M. 2018 Remediation techniques for heavy metal-contaminated soils: principles and applicability. *Science of the Total Environment* **633**, 206–219.

Makino, T., Maejima, Y., Akahane, I., Kamiya, T., Takano, H., Fujitomi, S., Ibaraki, T., Kunhikrishnan, A. & Bolan, N. 2016 A practical soil washing method for use in a Cd-contaminated paddy field, with simple on-site wastewater treatment. *Geoderma* **270**, 3–9.

Matouq, M., Jildeh, N., Qtaishat, M., Hindiyeh, M., Maha, Q. & Syouf, A. 2015 The adsorption kinetics and modeling for heavy metals removal from wastewater by *Moringa* pods. *Journal of Environmental Chemical Engineering* **3** (2), 775–784.

Meunier, N., Laroulandie, J., Blais, V. F. & Tyagi, R. D. 2003 Cocoa shells for heavy metal removal from acidic solutions. *Bioresource Technology* **90** (3), 255–263.

Mohapatra, M., Khatun, S. & Anand, S. 2009 Kinetics and thermodynamics of lead (II) adsorption on lateritic nickel ores of Indian origin. *Chemical Engineering Journal* **155** (1–2), 184–190.

Onotri, L., Race, M., Clarizia, L., Guida, M., Alfè, M., Andreozzi, R. & Marotta, R. 2017 Solar photocatalytic processes for treatment of soil washing wastewater. *Chemical Engineering Journal* **318**, 10–18.

Panda, L., Rath, S. S., Rao, D. S., Nayak, B. B., Das, B. & Misra, P. K. 2018 Thorough understanding of the kinetics and mechanism of heavy metal adsorption onto a pyrophyllite mine waste based geopolymer. *Journal of Molecular Liquids* **263**, 428–441.

Petrou, A. L. 2012 The free energy of activation as the critical factor in geochemical processes. *Chemical Geology* **308–309**, 50–59.

Petrou, A. L. & Economou-Eliopoulos, M. 2009 Platinum-group mineral formation: evidence of an interchange process from the entropy of activation values. *Geochimica et Cosmochimica Acta* **73** (19), 5635–5645.

Radi, S., El Abiad, C., Moura, N. M. M., Faustino, M. A. F. & Neves, M. G. P. M. S. 2017 New hybrid adsorbent based on porphyrin functionalized silica for heavy metals removal: synthesis, characterization, isotherms, kinetics and thermodynamic studies. *Journal of Hazardous Materials*. https://doi.org/10.1016/j.jhazmat.2017.10.058.

Safarik, I., Horska, K., Svobodova, B. & Safarikova, M. 2012 Magnetically modified spent coffee grounds for dyes removal. *European Food Research and Technology* **234** (2), 345–350.

Saini, A. S. & Melo, J. S. 2013 Biosorption of uranium by melanin: kinetic, equilibrium and thermodynamic studies. *Bioresource Technology* **149**, 155–162.

Silva, M., Nebra, S., Silva, M. M. & Sanchez, C. 1998 The use of biomass residues in the Brazilian soluble coffee industry. *Biomass and Bioenergy* **14** (5–6), 457–467.

Suresh, S., Karthikeyan, S. & Jayamoorthy, K. 2016 FTIR and multivariate analysis to study the effect of bulk and nano copper oxide on peanut plant leaves. *Journal of Science: Advanced Materials and Devices* **1** (3), 343–350.

Tohdee, K., Kaewsichan, L. & Asadullah, 2018 Enhancement of adsorption efficiency of heavy metal Cu(II) and Zn(II) onto cationic surfactant modified bentonite. *Journal of Environmental Chemical Engineering* **6**, 2821–2828.

Tran, H. N., You, S. J. & Chao, H. P. 2016 Thermodynamic parameters of cadmium adsorption onto orange peel calculated from various methods: a comparison study. *Journal of Environmental Chemical Engineering* **4** (3), 2671–2682.

Usman, A. R. A. 2008 The relative adsorption selectivities of Pb, Cu, Zn, Cd and Ni by soils developed on shale in New Valley, Egypt. *Geoderma* **144** (1–2), 334–343.

Virjayaghavan, K., Teo, T. T., Balasubramanian, R. & Joshi, U. M. 2009 Application of *Sargassum* biomass to remove heavy metals from synthetic multi-metal solutions and urban storm water runoff. *Journal of Hazardous Materials* **164** (2–3), 1019–1023.

Wang, J., Zhao, Y., Zhang, P., Yang, L., Xu, H. & Xi, G. 2018 Adsorption characteristics of a novel ceramsite for heavy metal removal from stormwater runoff. *Chinese Journal of Chemical Engineering* **26**, 96–103.

Weber, W. J. & Morris, J. C. 1963 Kinetics of adsorption on carbon from solution. *Journal of the Sanitary Engineering Division* **89** (2), 31–60.

Wei, M., Che, J. & Wang, X. 2016 Removal of arsenic and cadmium with sequential soil washing techniques using Na_2EDTA, oxalic and phosphoric acid: optimization conditions, removal effectiveness and ecological risks. *Chemosphere* **156**, 252–261.

First received 4 October 2018; accepted in revised form 22 February 2019. Available online 5 March 2019